# Adhesive, self-healable and biodegradable dopamine modified PVA films for sustainable electronics

Monisha Monisha[a], Monisha Anand[b], Sagarika Panigrahi[c], Michael Vedel Wegener Kofoed[b], Ramin Aghababaei[d], Shweta Agarwala[a*]

[a] Electrical and Computer Engineering Department, Aarhus University, 8200 Aarhus, Denmark.

[b] Microbial Conversion Technologies, Department of Biological and Chemical Engineering, Industrial Biotechnology, Aarhus University, Gustav Wieds Vej 10 C, 8000 Aarhus, Denmark.

[c] Department of Civil Engineering, National Institute of Technology Agartala, Tripura, India,

[d] Department of Mechanical and Production Engineering, Aarhus University, 8200 Aarhus, Denmark.

*shweta@ece.au.dk

**Abstract**. The potential of sensing devices can be significantly enhanced by utilizing biodegradable polymers with adjustable mechanical, adhesion, and healing properties. In this study, adhesive films made from dopamine (DA) and citric acid (CA) modified polyvinyl alcohol (PVA) are presented. These films are exclusively derived from bio-based materials, following an environmentally friendly and easily reproducible process that is also scalable. They exhibit robust adhesion and easy detachment from various substrates, such as stainless steel (138 – 191 kPa), particularly in the presence of moisture. In contrast to the extended degradation time of pure PVA, the composite films prepared in this study show accelerated degradation under anaerobic conditions. Notably, modified biofilms (P1DA1CA1, P1DA2CA1) exhibit superior degradation compared to conventional plastic PVA, with the exception of P1DA1CA2. The slower degradation in P1DA1CA2 is attributed to the higher acidic concentration contributed by citric acid. The study delves into the morphological changes of the prepared and degraded films using scanning electron microscopy (SEM), and

the degradation process is characterized through chromatographic techniques. The study suggests that dopamine (DA) and citric acid (CA) molecules penetrate the interplanar distance of P chains, as supported by powder X-ray diffraction studies, thereby expediting the degradation process. Additionally, the inclusion of CA enhances the stability of DA molecules against oxidation, increases H-bonding, and acts as a plasticizer. These synergistic interactions are further corroborated by Fourier transform infrared (FTIR), SEM, thermogravimetric analysis (TGA), and tensile studies. The introduction of DA and CA imparts self-healing properties to the films due to the presence of multiple H-bonds. Tensile studies reveal that the strength of self-healed samples approaches that of pristine samples. Overall, the findings of this study hold promise for the development of innovative, biodegradable PVA-based self-healing adhesive films with potential applications across various domains.

## 1. Introduction

The global focus on addressing the escalating issue of electronic waste (e-waste) has prompted a concerted effort to identify sustainable solutions within the electronics industry. A primary focus of this endeavor involves the development and design of biodegradable materials with diverse electronic functionalities. The insulating substrate, a key component of electronic circuits occupying a substantial area, has drawn particular attention. Consequently, the research community is actively exploring sustainable alternatives to traditional non-degradable substrates like epoxy resin, glass fabric composites, and indium-tin-oxide glass.

It is essential to note that the aforementioned substrates lack adhesive properties. Despite the strides made in producing biocompatible or biodegradable materials with variable adhesive characteristics, these efforts have predominantly centered around biomedical applications. The challenge remains to identify robust adhesives that perform well in both wet and dry environments. In pursuit of this goal, researchers have turned to nature for inspiration, creating biomimetic adhesives that mimic the adhesive abilities of beetles, geckos' feet, and marine

mussels.[1,2] These synthetic, nature-inspired adhesives have not only shown promise in providing strong adhesion but have also contributed to the development of biodegradable and transient systems. This advancement holds potential for closing the loop on electronic waste generation. However, it is worth noting that the raw materials typically employed in fabricating self-adhesive and biodegradable devices, such as silk or human proteins like fibrin, impact the availability and cost of the final product. As a result, these options may not be deemed industrially viable.[3,4]

For fabricating a self-adhesive, economically viable and biodegradable film-based substrate, dopamine (DA) is a promising choice. It has been explored for the first time by Tanzer *et al*. in 1981.[5] It is an amino acid, 3,4-dihydroxyphenylalanine, found in human body and as a constituent in adhesive proteins of marine mussels. Marine mussels have attracted huge attention in the last years due to their incredible ability to stick to various organic and inorganic substrates in harsh environments. Very few studies report the use of dopamine for adhesion because in solution it undergoes rapid oxidative self-polymerization to polydopamine (PDA).[6] However, there has been many reports mentioning use of PDA as coatings,[7,8] self-healing,[9-11] self-adhesives,[11,12] corrosion[13] and antifouling applications.[14-16] Therefore, distinct polymeric biomaterials bearing catechol moieties have been developed trying to mimic this incredible adhesive performance.[17-20] However, PDA has less adhesion as compared to unoxidized DA due to the involvement of its functional groups responsible for adhesion in polymerization process.[21] For the same reason, there has been many reports for different polymerization methods of DA under variable conditions for the purpose of regulating the particle size and stability which in turn effects the adhesion of PDA.[22]

The adhesive properties of PDA or catechol based molecules have been investigated majorly in the form of hydrogel or glues for biomedical applications in combination with chitosan,[19] hyaluronic acid,[23] urethanes,[18] fibrin glue[24] etc using blending,[25] crosslinking chemistry,

[26] clickable coupling reactions[27] or multiplex supramolecular interactions.[28] The use of expensive raw materials or tedious preparation methods limited their practical applications. Hence, there is a need to simplify the preparation process to scale up the production at low cost. So far, no one has reported the fabrication of a material which shows dual properties of acting as a substrate for printed electronics as well as adhesion to various types of materials.

Moreover, technologies for safe disposal of electronics have rarely been explored and eventually they end up as electronic waste in landfills. Most designs neglect these important aspects of devices, hindering them from real-world applications. Despite the successful integration of self-adhesiveness, toughness and stretchability, these adhesive materials did not show very good transparency due to the presence of brown colored PDA.[29] Only few attempts were made to assimilate transparency with other properties such as healing ability, mechanical strength, adhesiveness, and biodegradability in a single system.[30] This is extremely desirable for the development and utilization of next-generation eco-friendly devices.

Furthermore, there has been limited exploration of technologies for the safe disposal of electronics, leading to their eventual accumulation as electronic waste in landfills. Many device designs overlook these crucial aspects, impeding their practical applicability in the real world. While some materials have successfully integrated self-adhesiveness, toughness, and stretchability, their transparency is compromised by the presence of brown-colored PDA.[29] Efforts to reconcile transparency with other essential properties, such as healing ability, mechanical strength, adhesiveness, and biodegradability within a single system, have been scarce.[30] Achieving this amalgamation is crucial for the development and utilization of next-generation eco-friendly devices.

The biodegradability of polymers can be assessed through either aerobic or anaerobic treatment methods. Among these, anaerobic digestion (AD) stands out as one of the most extensively

employed techniques. Anaerobic digestion involves a process without oxygen and finds widespread application in the treatment of industrial, agricultural, and municipal waste. Notable advantages of the AD process include its low energy demand, generation of smaller biomass quantities, minimal nutrient requirements, and the utilization of digestate as fertilizer. The AD process has also been employed to evaluate the biodegradability of PVA. (Gartiser et al., 1998; Matsumura et al., 1993; Russo et al., 2009; Sitthi et al., 2022; Zhang et al., 2010) and different type of modified polymers (Gartiser et al., 1998, 1998; Matsumura and Tanaka, 1994; Mohee et al., 2008; Russo et al., 2009; Sitthi et al., 2022). Hence in the present study, to check the biodegradability of the films a batch AD experiment along with kinetic analysis was conducted.

This study introduces an innovative approach to instill adhesive properties into a biodegradable substrate for potential use in electronic device fabrication. The authors employed a one-pot reaction to fabricate multifunctional polymeric composite films (PxDAyCAz) with a range of distinctive properties. These properties encompass intrinsic viscoelasticity, tunable mechanical strength, self-adhesiveness, self-healability, and biodegradability. The fabrication involved mixing a polyvinyl alcohol (P) solution with dopamine (DA) and citric acid (CA), resulting in an interpenetrating network of multiple noncovalent interactions. The abundant inter- and intramolecular hydrogen bonds within the matrix confer viscoelastic behavior to the composite films, making them suitable for environmentally acceptable applications. The presence of numerous catechol groups on DA imparts self-adhesiveness to the films in the presence of moisture, enabling adhesion to various surfaces, both organic and inorganic. The exposed surface of the film, non-sticky and hydrophilic, proves compatible with water-based inks for printing applications. The films, characterized by numerous noncovalent interactions, exhibit rapid and durable self-healing abilities. This comprehensive set of properties positions the composite films as promising candidates for a wide range of applications in electronic device

manufacturing. Consequently, a batch AD experiment, coupled with kinetic analysis, was conducted to examine the biodegradability of the films. The anaerobic digestion (AD) process was utilized in the current study to assess the biodegradability of PVA.

## 2. EXPERIMENTAL SECTION

**2.1 Materials**. PVA (P, Mw 89,000-98,000, 99+% hydrolyzed), dopamine hydrochloride (D), citric acid (C) and Tris-buffer (pH 7 and 8.5) were obtained from Sigma-Aldrich and used as received without further purification. Stainless steel 304 and polytetrafluoroethylene (PTFE) plates were obtained from TriboTonic.

**2.2 Characterization**. Fourier transform infrared (FTIR) spectra were recorded on a Nicolet iS5 FTIR spectrometer equipped with an attenuated total reflectance diamond accessory (iD5-ATR) in the range 4000-400 $cm^{-1}$. Thirty-two scans were recorded and referenced against the empty ATR device without a sample. The ultraviolet–visible (UV–vis) spectra were recorded using Calriostar plate reader spectrophotometer. The morphologies of composite films were characterized by scanning electron microscope (SEM) using FEI Magellan 400 SEM. To enhance the quality of the images', samples were coated with 10 nm Ti coating using Cryofox Explorer 500 GLAD. The volatile fatty acids (VFA) were measured by gas chromatography (GC, Agilent Technologies, United States 7890 A GC system with FID). The biogas produced was analyzed using GC (Agilent Technologies United States with TCD using Helium as carrier gas). TGA of starting materials and composite films was performed with Mettler Toledo in the temperature range 30 to 800 ºC and a heating rate of 10 ºC/min under a nitrogen atmosphere at a flow rate of 50 mL/min. Adhesion performance was investigated according to ASTM D1002 by measuring the lap shear strength (LSS) of the composite films to steel and PTFE. Zwick Roell tensiometer was used with a 500 N load cell at a crosshead speed of 1.3 mm/min. Specimens were prepared by applying films after dipping in DI water or 10% solution of P, DA and CA with the same weight ratio as films to the sample surface with the bonding area of

2 cm × 1.3 cm. The total thickness of the adhesive layer was maintained in the range of ~ 0.2 - 0.4 mm for films and ~ 0.05–0.1 mm for solution. Prepared samples were dried overnight in hot air oven at 50 ºC before performing the experiment to ensure effective drying and adhesion of the films to the substrate. Testing was carried out in triplicate and the average value along with the standard deviation was reported. To measure the tensile strength of as prepared films, samples were cut into 4 cm × 1 cm strips and stretched with a load of 500 N at a crosshead speed of 5 mm/min. Same procedure was repeated for self-healed films. Experiments were performed in triplicate for each film and the average value along with the standard deviation was reported.

**2.3 Fabrication of films**. PVA (P) powder (300 mg) was dissolved in deionized water (10 mL) and stirred magnetically at high speed (~1000 rpm) at 90 ºC till a clear 3% solution was obtained. This P solution was allowed to cool down to room temperature. To the above solution, first citric acid (CA) was dissolved followed by dopamine (DA) and the resulting solution was further stirred at room temperature for 1 h to homogenize. The so-formed solution was then poured into silicon mold (4 cm × 4 cm × 1 cm) and dried at 45 ºC to form a thin composite film. The samples were abbreviated as $P_xDA_yCA_z$, where x, y and z are the weight ratios of P, DA and CA in the formed film. The P:DA:CA feed ratio was varied as 1:1:1, 1:2:1 and 1:1:2 and therefore, the resultant samples were abbreviated as $P_1DA_1CA_1$, $P_1DA_2CA_1$, $P_1DA_1CA_2$, respectively. To check the effect of CA as a plasticizer and stabilizer for DA, a solution was prepared without CA ($P_1DA_1$). As expected, the formation of a non- flexible and brown colored film was observed upon drying of the solution as can be seen in **Fig. S1a-b**. pH of the prepared solutions with variable feed ratios of CA and DA are given in **Table S1**. It was observed that different loading of DA and CA affect the texture of the film. The film surface became smoother with an increase in the amount of CA, which can be attributed to its

plasticization effect. Whereas the high loading of DA did not allow formation of smooth films as shown in **Fig. S2b**.

**2.4 Swelling Behavior and Gel content**. Equilibrium water swelling of composite films was evaluated by measuring water uptake by films. ~ 100 mg of each film was immersed in 5 ml of DI water at room temperature. The amount of water absorbed was measured after regular intervals of time until the weight of the swollen samples remained constant. The equilibrium water absorption (EWA, %) of films was measured using equation 1. After swelling measurements, the samples were dried in oven at 70 °C for 24 h. Gel content (GC) was measured using eq 2.

$$EWA = \left(\frac{W_s - W_i}{W_i}\right) \times 100 \qquad (1)$$

$$GC(\%) = \frac{W_f}{W_i} \times 100 \qquad (2)$$

where $W_s$ is the weight of the swollen sample, $W_i$ is the initial weight and $W_f$ is the final weight of the dried sample.

**2.5 Anaerobic degradation**. The anaerobic biodegradability of four different films P, $P_1DA_1CA_1$, $P_1DA_2CA_1$, $P_1DA_1CA_2$ was investigated by batch anaerobic digestion (AD) study. The batch AD experiment was conducted by water displacement method (ASTMD5526-94d). The inoculum was collected from the AD plant treating animal manure and straw running inside the Aarhus University campus. The films of P, $P_1DA_1CA_1$, $P_1DA_2CA_1$, $P_1DA_1CA_2$ were cut into ~ 2 cm × 2 cm. The samples were analyzed in duplicate, and one set was assessed without addition of any test material and considered as control. Around 200 mL of inoculum, 8g of P, 4g of $P_1DA_1CA_1$, $P_1DA_2CA_1$, $P_1DA_1CA_2$ were added in four different digestion bottles. The proportion of polymer and inoculum was selected to provide sufficient microbial attack to polymers. The films $P_1DA_1CA_1$, $P_1DA_2CA_1$, $P_1DA_1CA_2$ were washed before adding into the

digestion bottle to eliminate the acidic condition caused by citric acids present on the surface of polymer. The schematic diagram and original image of digestion setup is given in **Fig. 1**. After adding the polymer films to the inoculum, volatile fatty acids (VFA) and pH of the mixture was measured followed by sealing the bottles by using gas tight rubber stopper and crimping by an aluminium ring. The biogas produced during the experiment was analyzed using Gas Chromatography (GC) at regular intervals of time and the cumulative amount of generated gas was used to calculate the amount of degradation of composite films. At the end of the experiment VFA was measured by GC and pH was recorded.

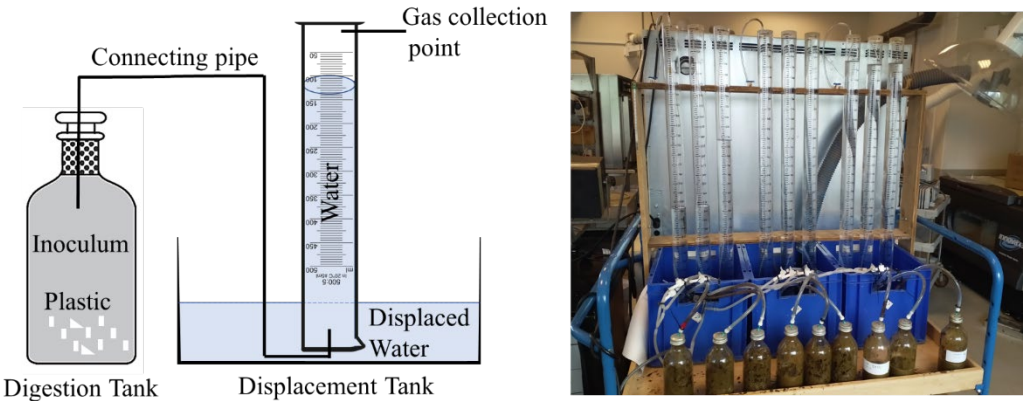


**Fig. 1**. (a) Schematic diagram and (b) original image of anaerobic digestion setup.

**2.6 Evaluation of self-healing behavior**. The composite films were cut into 4 cm × 1 cm strips. Each strip was further cut into half. For self-healing, the cut specimens were then joined together by overlapping ~1 mm of the cut surface wetted with water and kept at the same position for 1 h at 50 ºC to heal and to ensure complete removal of water. Tensile measurements of healed samples were carried out in triplicates.

**2.7 Kinetic Analysis**. To forecast methane production and assess the bio-kinetic parameters, the study used modified Gompertz model computational model. In order to estimate these parameters from experimental data on cumulative methane yield, nonlinear least-square

regression analysis was carried out in MS Excel using the solver tool. Reducing the difference in methane output between measured and simulated values was the objective. The models were evaluated using statistical metrics like the coefficient of determination (R2) and root mean square error.

Modified Gompertz model: $Y = M * exp\left\{-exp\left[\frac{R_m \cdot e}{M}(\lambda - t) + 1\right]\right\}$ ..... Eq. 1

Logistic Function Model: $Y = M * \{1 - \exp(-\frac{Rm(t-\lambda)}{M}\}$..... Eq. 2

Transference function model = $\frac{M}{1+\exp\{\frac{4\,Rm\,(\lambda - t0}{M}+2\}}$ ..... Eq. 3

Where,

Y = Cumulative experimental methane yield (mL/gVS$_{added}$),

M = Ultimate methane yield (mL/gVS$_{added}$),

Rm = Maximum methane production rate (mL/gVS d),

λ = Lag phase time(d), and

e = exp (1) = 2.7183.

The statistical indicators used to evaluate the accuracy of the models were:

(i) The coefficient of determination (R2), a measure of the degree of similarity between measured and predicted methane yield values. R2 values range from 0 to 1, where a value of 0 indicates that the model does not explain any variance in the dependent variable and a value of 1 indicates that the model fully explains the variance in the dependent variable. When the model's R2 value is close to 1, it indicates a strong relationship between the independent variable(s) and the dependent variable and can be used to forecast methane production with accuracy. The mean square error, or root mean square error, is calculated as the average of the squares of the deviations between the measured and anticipated values of methane yield. It is used as a metric to measure the accuracy of predictions or estimates.

Root means square error = $\sqrt{\sum_{i=1}^{n} \frac{(PMY_i - EMY_i)^2}{n}}$ ..... (4)

Where,

$PMY_i$ is the Predicted methane yield for ith day of measurement,

$EMY_i$ is the experimental methane yield for ith day of measurement, and

n = it is the number of measurements.

## 3. RESULTS AND DISCUSSION

The multifunctional composite films with self-adhesive, self-healable, and biodegradable properties were fabricated by drying a simple solution of PVA (P), dopamine (DA) and citric acid (CA) (**Scheme 1**). The fabrication procedure was benign to the environment and did not involve the usage of any organic solvent and purification step. Since it is known that DA has better adhesive properties as compared to polydopamine, film fabrication using DA demands exploration of a processing strategy which can prevent its oxidative polymerization.[31] One of the methods to achieve this is covalent linking of DA with polymer chains.[30] In our case, incorporation of CA improved the adhesion of prepared films by enhancing their flexibility without any requirement of chemical crosslinking of DA to P (**Fig. S1c**). CA was used for dual purposes. (1) It acts as a plasticizer. Thus, it gave flexibility to the films and helped in holding DA within the P matrix through H-bonding. (2) DA is highly susceptible to oxidative polymerization in the presence of oxygen and basic conditions (pH = 8.5).[6] CA impeded the polymerization of DA by making the pH of the solution acidic.[32] As a result, the so-formed films were white in color contrary to the previously reported studies where due to the polymerization tendency of DA, prepared products were black or darker in color (**Fig. S1**).[29] This multifaceted benefit of introduction of CA with being biodegradable enables it as a promising stabilizer for the film fabrication. However, efficient packing of P chains due to intrinsic inter and intramolecular H-bonding between hydroxyl groups demands prior

disruption to favor their co-interaction with DA and CA. This was achieved by solubilizing P powder in DI water at 90 ºC at high speed (~ 1000 rpm) until a clear solution was obtained. Since DA and CA have free -OH, -$NH_2$ and -COOH functionality respectively, they can interact with P and with each other through H-bonding.

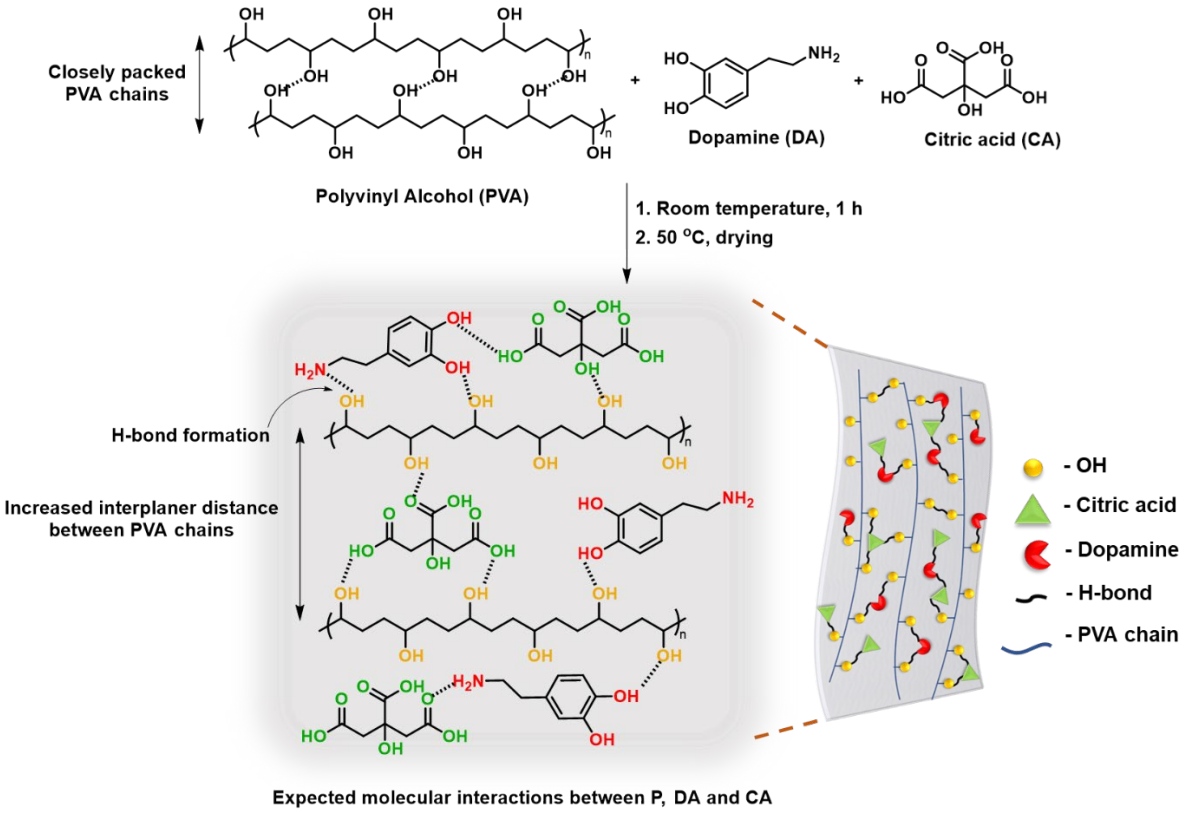


***Scheme 1***. *Synthetic strategy followed to prepare composite films $P_xDA_yCA_z$.*

There are numerous studies showing different conditions under which DA polymerization occurs. The process is rapid in the presence of oxygen and alkaline environment (pH ~8.5). [7,33,34] Removal of oxygen can slow down the polymerization process but does not inhibit it completely. Also, it has been reported that hydroxyl (·OH), singlet oxygen ($^1O_2$), superoxide ($O_2^{-\cdot}$) and peroxide ($O_2^{2-\cdot}$) radicals are required by dopamine for self-polymerization.[33,35,36] Therefore, Du and co-workers demonstrated that UV irradiation (260 nm) can be used on dopamine solution in presence of oxygen to accelerate the polymerization process under acidic,

basic or neutral conditions. As expected, the kinetics of polymerization was slowest under acidic environment (pH ~1).[33] Tung-Po Chen *et al*.[22] successfully carried out polymerization of DA in plasma activated water under acidic pH (< 5.5) in the absence of oxygen. Since DA has better adhesion than polydopamine,[21] taking into account the above studies, the present research avoided the conditions favorable for polymerization by making the pH of the solution acidic using CA. No polymerization of DA was observed in solutions prepared for film fabrication over a period of 2 months (**Fig. 2a- i to iii and 2b- i to iii**). DA solution in presence of P ($P_1DA_1$) started to polymerize within 1 h and significant color change was observed after 24 hours (**inset of Fig 2b-iv**). While pure DA solution (**Fig. 2b-v**) showed slower kinetics towards polymerization. The change was more prominent in $P_1DA_1$ solution attributed to the increase in pH (6.19) due to the presence of P. As expected, upon removal of P, a solution of (CA + DA) owing to the decrease in pH (2.31) remained stable for over 2 months as shown in **Fig. 2a-vi**.

In order to verify that DA is not polymerizing in the optimized conditions, UV-vis spectra of solutions (1 mg/mL) were measured at room temperature. The experiment was performed using DI water, and buffer solutions at pH 8.5 and pH 7 (Tris buffer). It discovered that pure DA solution in DI water did not show any change in UV-vis spectra for up to 3 days since the pH of solution was 4.89 (**Fig. S3**). However, DA showed polymerization within 5 minutes after mixing with a buffer solution of pH 8.5 as indicated by rapid solution color change. Spectra showed drastic change in 3 days with a broad absorption because of the formation of a series of intermediate products in the process of polymerization (**Fig. 2c**).[37] In presence of CA, reaction slowed down and a shoulder at 300 nm appeared in the UV-vis spectrum. The changes can be traced better at pH 7 due to the slow polymerization process (**Fig 2d**). In all the solutions, it was observed that addition of CA along with DA either inhibited or slowed down the

polymerization process. These results indicate that decrease in pH slows down the polymerization process irrespective of the presence of oxygen.

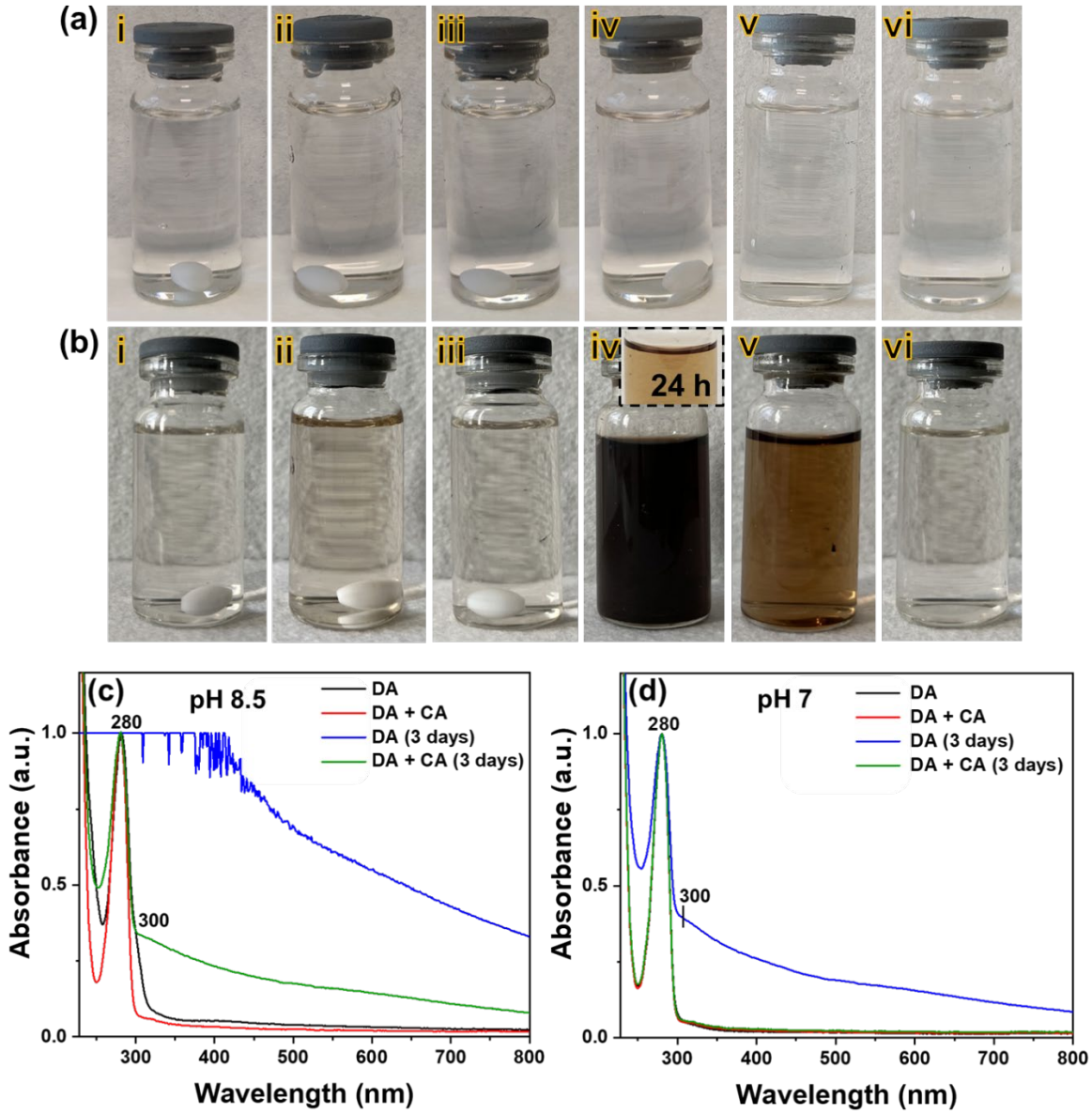


***Fig. 2***. *Optical images showing stability of solutions with and without CA on (a) day 1 and (b) over a period of two months. i, ii, iii and iv are the solutions for films* $P_1DA_1CA_1$, $P_1DA_2CA_1$, $P_1DA_1CA_2$ *and* $P_1DA_1$, *respectively. v and vi are solutions of DA and DA + CA in water, respectively. Inset in b- iv is showing the change in color of* $P_1DA_1$ *due to polymerization after 24 h. Stability of DA through UV-vis studies in absence and presence of CA at (c) pH 8.5 and (d) pH 7.*

**Network structure of composite films**. To develop understanding of physical interactions among P, DA and CA in the films, a systematic analysis by FTIR, swelling behavior, XRD spectroscopy and SEM was performed.

**FTIR Analysis**. The chemical structure was characterized by FTIR spectroscopy (**Fig. 1a** and **b**). The presence of characteristic peaks of DA at 1616-1582 $cm^{-1}$ (-$NH_2$, C=C), 1284 $cm^{-1}$ (-CO) and 815 $cm^{-1}$ (-$NH_2$, -CN) demonstrated its presence in the composite films. The spectra of composite films showed noticeable differences as compared to the starting materials. The blue shift of the broad -OH band of P (from 3284 $cm^{-1}$ to 3320 $cm^{-1}$), merging and broadening of carbonyl peaks of citric acid (from 1741 and 1691 $cm^{-1}$ to 1705 $cm^{-1}$) and broadening of -$NH_2$ (~3339 $cm^{-1}$) and -OH (1188-1144 $cm^{-1}$) peaks of DA in composite films indicated the inter and intra-molecular H-bonding interaction in between hydroxyl, amine and carbonyl functionalities of P, DA and CA, respectively. The presence of these dynamic linkages is conducive to fracture, self-healing and homogenization of the network under stress.

**Swelling behavior**. The degree of crosslinking density of composite films was qualitatively studied by measuring the EWA (eq. 1) with the immersion of films in water and by measuring the GC. The obtained values are reported in **Table S2**. There was no more uptake of water after 2 days (**Fig. 3c**). This is due to the attainment of equilibrium and transformation of films into very soft gels (**Fig. 3d**). This made the removal of excess water from the surface of gels difficult as they were leaving traces on the blotting paper and thus a decrease in water absorption was observed. Higher EWA of composite films as compared to P (~140%) indicated loose packing of P chains in the films due to the intercalation of DA and CA molecules and increase in the number of polar functional groups which was highest in film $P_1DA_1CA_2$.[18] The GC of P film was highest (~ 94%) which demonstrated high crosslinking or tight packing of P chains. Whereas due to the loosely packed P chains and free DA and CA molecules, GC of composite films reduced by ~ 63% - 76% as compared to P film.

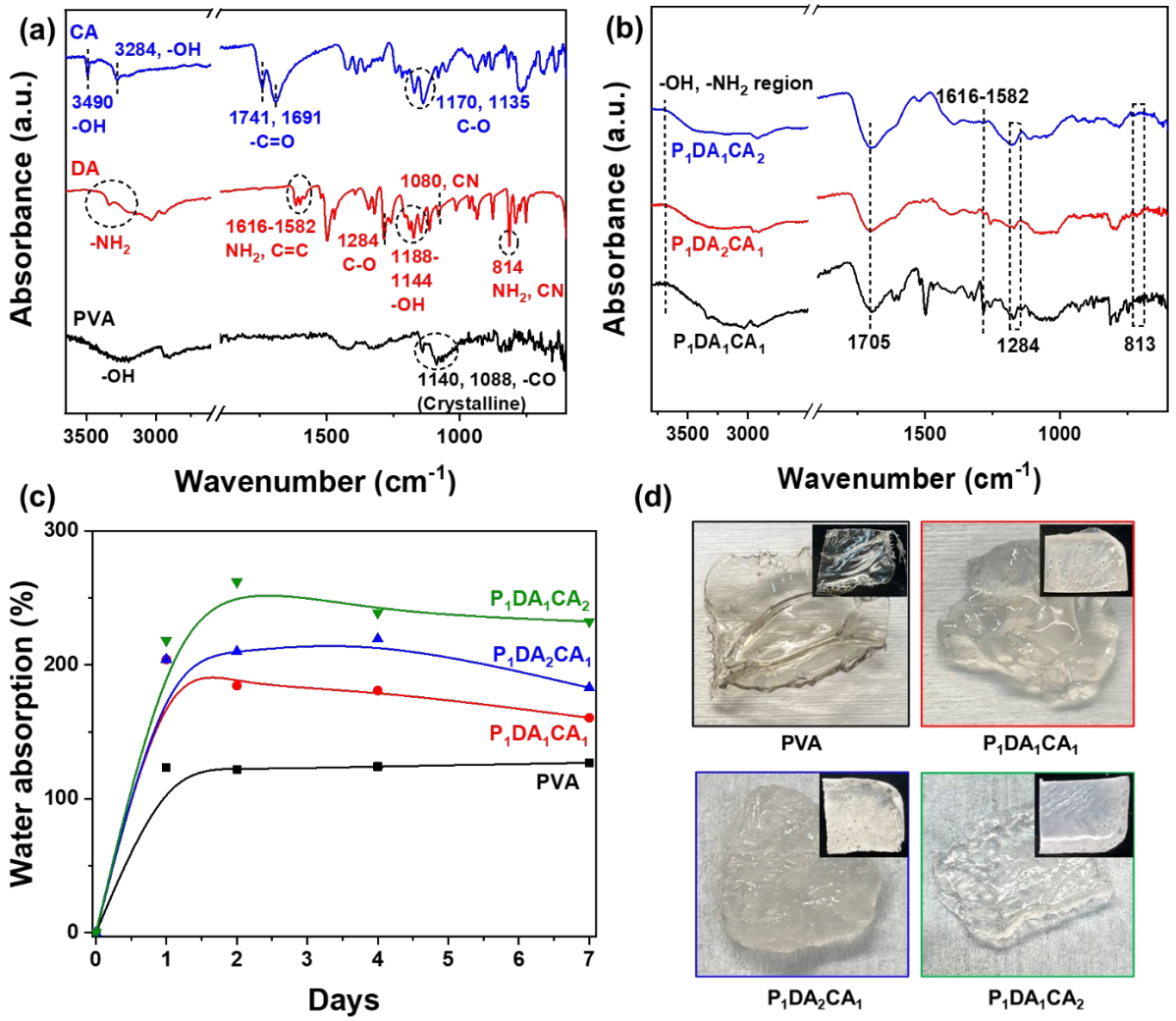


***Fig. 3****. Stacked FTIR spectra of (a) the raw materials P, DA and CA, and (b) composite films-* $P_1DA_1CA_1$, $P_1DA_2CA_1$, $P_1DA_1CA_2$. *(c) Equilibrium water absorption (EWA) of composite films and (d) optical images of swollen films at the end of the experiment.*

**XRD Analysis**. Changes in crystallinity of P were ascertained by X-ray diffraction spectroscopy. The peak located at 2θ = 19.75° and 21.94° were attributed to the crystalline diffraction and, inter- and intra-molecular H-bonding of pure P.[38,39] With the incorporation of DA and CA, decrease in the intermolecular H-bonding in between P chains and increase in the intramolecular H-bonding between P, DA and CA lead to the decrease in crystallinity. This can be seen by the broadening of crystalline peaks of P in composite films. In films, changes in the pattern of DA and CA spectra such as occurrence of new peak and disappearance of some peaks

suggested formation of new linkages between P, DA and CA (**Fig. S4**). This accounted for the disruption in the orderly arrangement of P chains in an irregular fashion.

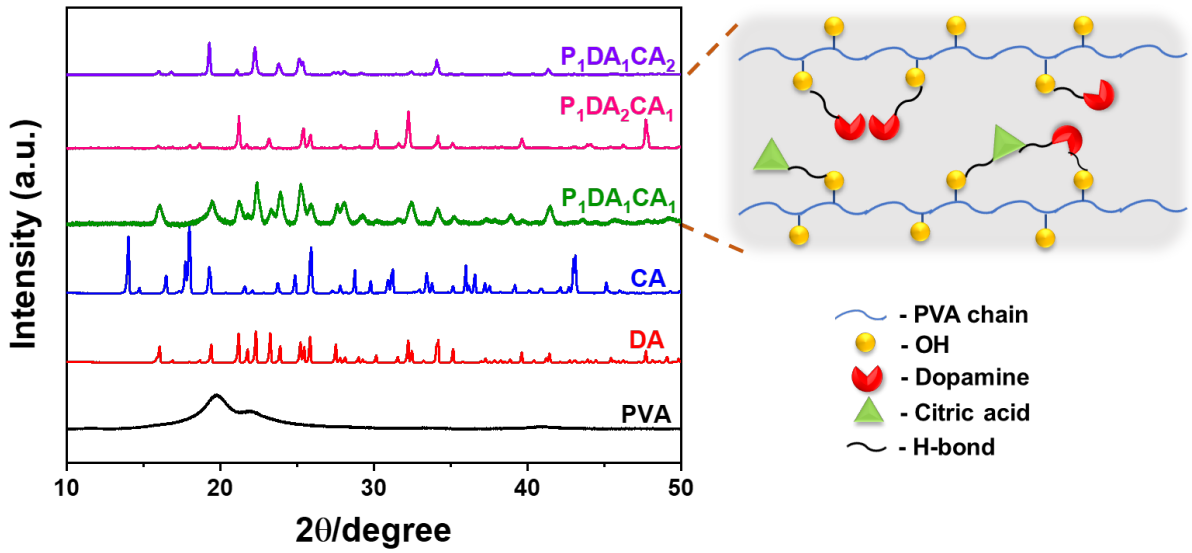


***Fig. 4****. XRD patterns of P and composite films at room temperature. Probable structural organization of DA and CA molecules across P polymer backbone.*

**SEM Analysis**. SEM was performed to study the morphological changes in microstructure of P film upon introduction of different loadings of DA and CA (**Fig. 5**), and degradation induced surface changes after keeping the films in sludge for 2 months. SEM micrographs of composite films revealed a significant effect of incorporation of DA and CA in P. The extensive H-bonding in P film contributes to an ordered arrangement of P chains and thus imparting an even morphology without features of surface roughness (**Fig. 5a-i**). Physical interactions of DA and CA via H-bonding resulted in a remarkable change in the morphology of films. Increase in content of DA enhanced the morphological roughness of P film by disrupting the H-bonding network of P chains in a random fashion. In addition, the appearance of spherical nanoparticles on the surface of composite films can be assigned to aggregates of DA and CA as they cannot be seen in P film. However, reduced roughness and reduced number of nanoparticles in film with increase in amount of CA again supported the plasticization and stabilization effect of CA

due to the growth of intermolecular H-bonding network and interplanar placement of DA and CA in between P matrix. These results were in accordance with FTIR and XRD studies.

Rough surfaces increase the contact area between the microbes and the substrate. Thus, rough structure of films upon addition of DA enabled easy attachment of sludge bacteria (**Fig. S2**). SEM image of film $P_1DA_1CA_1$ indicated the maximum amount of degradation by showing development of porous structure. These changes were comparatively less in film $P_1DA_1CA_2$ and least in P film (**Fig. 5b**). As a result, modified films were responsible for higher methane production due to degradation than pure P film. Here, a point to be noted is film $P_1DA_2CA_1$ got completely dissolved in the sludge and could not extracted after completion of the studies for SEM characterization. This can be attributed to the presence of the irregular surface as compared to the other films under study which led to easy degradation and dissolution of film.

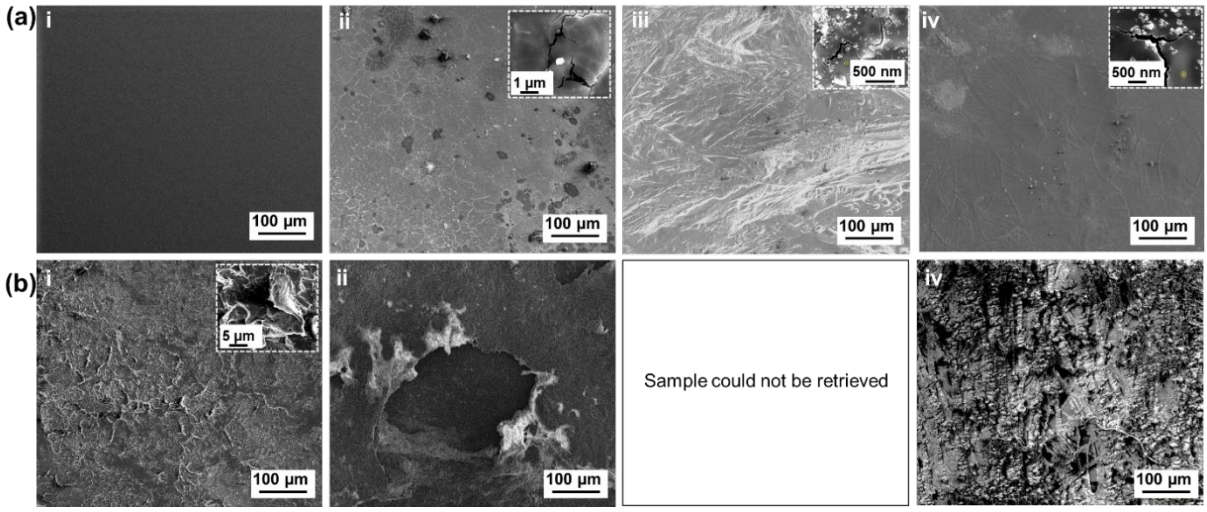


***Figure 5****. Representative SEM images of films (i)P, (ii) $P_1DA_1CA_1$, (iii) $P_1DA_2CA_1$ and (iv) $P_1DA_1CA_2$ before (a) as prepared and after (b) degradation.*

**TGA Analysis**. TGA was performed to investigate the thermal behavior of starting materials and composite films. TGA traces are shown in **Fig. 6** and the results are summarized in **Table**

**2**. Pristine P showed two step mass loss behavior. The initial mass loss at 269 ºC is attributed to the loss of side -OH groups and H-bonds. The second mass loss at 428 ºC corresponds to the main chain degradation. TGA curves suggest that the existence of variable inter-molecular H-bonding between P, DA and CA plays an important role in improving the thermal stability of the composite films above 300 ºC. Thermal stability was found to increase with an increase in DA content. For the same reason, there was an observed increase in char yield of $P_1DA_2CA_1$ film by 24.3%. To demonstrate the flame-retardant property of the polymer, limiting oxygen index (LOI) was determined. LOI above 26 is a good indicator of applicability of polymer for flame resistant applications. Despite the low LOI value of P and CA, the films showed good flame-resistant behavior which may be attributed to the incorporation of DA into the matrix. Thus, LOI value increased with increase in DA content.

**Table 2**. Comparison of thermal characteristics of composite films with P, CA and DA.

| Sample | P | DA | CA | $P_1DA_1CA_1$ | $P_1DA_2CA_1$ | $P_1DA_1CA_2$ |
|---|---|---|---|---|---|---|
| **Char Yield** | 2.5 | 17.9 | 0 | 23.4 | 26.8 | 23.4 |
| **LOI** | 18.5 | 24.6 | 17.5 | 26.9 | 28.2 | 26.9 |

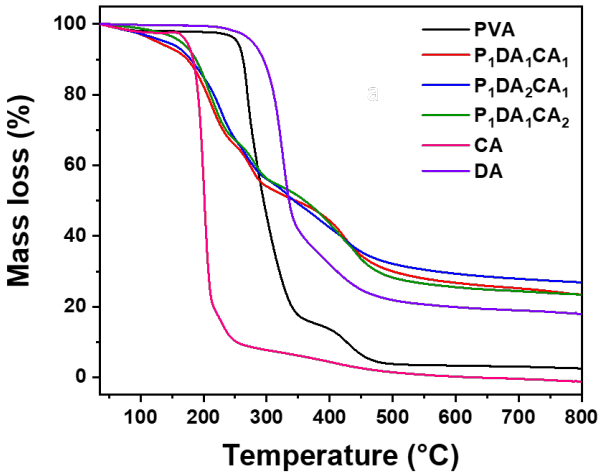


***Figure 6**. TGA profiles of $P_xDA_yCA_z$ composite films.*

**Self-healing**. Self-healing property in materials has gained interest as it is beneficial to improve the lifetime of materials and hence helps in reducing the environmental impact. Research on self-healing P has been mainly focused on hydrogels. However, in recent past there are a few research articles reporting self-healing of P based materials in film form.[9,40-43] As described above, the specimens were cut into two pieces. The films were found to self-heal when the cut surfaces were brought in contact with the help of water to heal at 50 °C for 1 h (**Fig. 7a**). The wet surface upon hydration becomes soft enough to make conformal contact with other films or adherend. Wet self-healing was mediated via self-assembly by interfacial H-bonding in between P and labile DA and CA moieties at the surface. **Fig. S5** shows that the healed films were well connected and retained flexibility.

To study the healing efficiency and its effect on mechanical properties of film, tensile strength of each healed film was measured and compared with pristine films. In most of the cases, samples did not tear apart from the fracture line which shows good self-healing was enabled by the formation of extensive DA and CA-mediated interfacial hydrogen bonding (**Fig. S6**). **Fig 7b** shows tensile strength of pristine and self-healed composite films. The tensile strength in both the cases was highest in film with maximum amount of CA since it provided homogeneity and flexibility to the films. The extended network of CA assisted hydrogen bonds can be attributed to dissipate energy efficiently to prevent crack propagation during stretching.[11] Therefore, we also observed maximum toughness and elongation in $P_1DA_1CA_2$ films (**Fig. S7**). The tensile strength was found to be least in $P_1DA_2CA_1$ film due to the inhomogeneity provided by increased amount of DA and hence lead to easy breakage of films. Interestingly, we did not observe very large differences between the tensile stress of pristine and self-healed films except in $P_1DA_2CA_1$ film which was 35%, 51% and 29% for $P_1DA_1CA_1$, $P_1DA_2CA_1$, and $P_1DA_1CA_2$ films, respectively. We anticipate that this difference can be further reduced by increasing the healing time to more than 1 h.

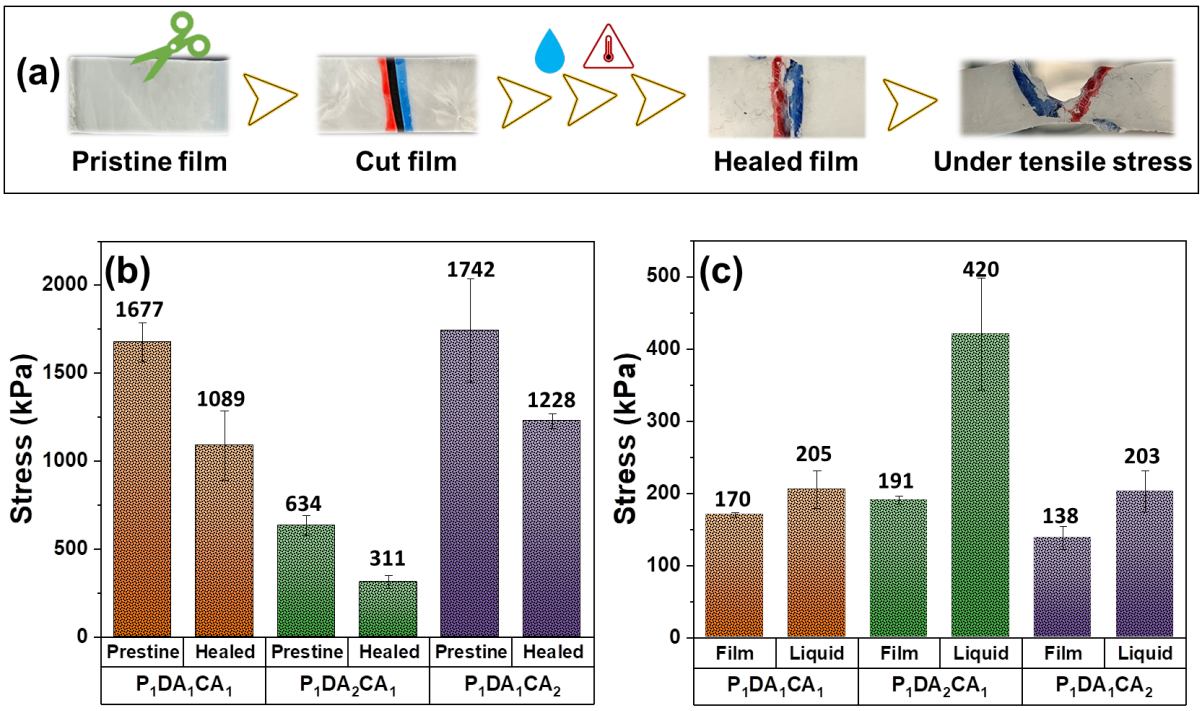


***Figure** 7. (a) Optical images showing self-healing process of film $P_1DA_1CA_1$ after cutting into two separate pieces and their behavior under tensile stress. (b) A comparison of mechanical strength of pristine and self-healed films. (c) A comparison of adhesion strength of films and 10% solution of P, DA and CA with the same weight ratio as films on steel lap joints.*

**Adhesion Performance**. One of the merits of our films is their strong adhesion to a wide range of surfaces. We tested the adhesion of $P_1DA_1CA_1$ film (0.5 cm × 4 cm) with the help of 50 g weight with glass, PTFE, metal, and wood surface (**Fig. S8**). We analyzed and compared the adhesion of films and in liquid form (10% solution of P, DA and CA with the same weight ratio as films) on steel and PTFE substrate using lap shear adhesion test. The films displayed distinct adhesion to steel substrates (138 kPa to 191 kPa) depending on the weight ratio of added DA (**Fig. 7c**). Owing to the more amount of DA, film $P_1DA_2CA_1$ has better adhesion as compared to the other two films. We could not further increase the amount of DA to find out the maximum achievable adhesion strength as large amount of DA inhibited the formation of a uniform film. Even in the present case also, the non-uniformity of $P_1DA_2CA_1$ film was large enough to affect the adhesion strength and therefore, it is very close to the $P_1DA_2CA_1$ film. To

confirm this, we checked the adhesion of films in liquid state also. As expected, owing to the more uniform distribution of liquid on the surface, solution of $P_1DA_2CA_1$ out-performed solution of $P_1DA_1CA_1$ and $P_1DA_1CA_2$ by 51% and 52%, respectively. To our surprise, we found that this solution was able to adhere PTFE substrates also (**Fig. S9**). However, because of the less adhesion strength even with liquid (67 – 93 kPa), we could not get any success to adhere PTFE joints with films under normal testing conditions without any external pressure. Thus, adhesion properties can be tuned by modifying the ratio of DA with respect to the other components used for film fabrication.

## 4. Batch anaerobic digestion of polymer

Batch AD of four different type of plastics were conducted for a period of 67 days to investigate the anaerobic biodegradability. The biogas production from the AD process indicates the degradation of polymer with time. The cumulative biogas yield of four different type of plastics (PVA, P1DA1CA1, P1DA2CA1, and P1DA1CA2) and the inoculum used for AD is presented in Fig. 2(a). Methane generation is largely dependent on the performance of anaerobic microorganisms growing in the anaerobic digester [1]. Table 1 provides an overview of the acquired bio-kinetic parameters (M, Rm and λ) and the statistical indicators (R2 and root mean square error) for the analyzed kinetic models. The transference function model exhibited the lowest root mean square error (1-35.1) and the highest R2 values (0.8782-0.9844), with the logistic function model following closely behind in terms of performance. Furthermore, it's important to note that the difference between the logistic function model and transference function model was not statistically significant ($P > 0.05$). In the logistic function model, the bio-kinetic parameter λ (lag phase) had a negative value, resulting in poor predictive accuracy for lag phase. The low error values (nearly equal to or less than 24%) obtained for transference function model suggests the applicability of model to predict the methane yield. The highest RMSE and lowest R2 was found for Modified Gompertz model, the bad results in data fitting

for Modified Gompertz model possibly because of the sigmoidal shape of the curve which well describe the phases of AD such as: lag, log and stationary. The Modified Gompertz model is mainly applicable for anaerobic digestion of lignocellulosic waste [1,2]. Hence in the present manuscript transference function model was used to analyse the bio-kinetic parameters.

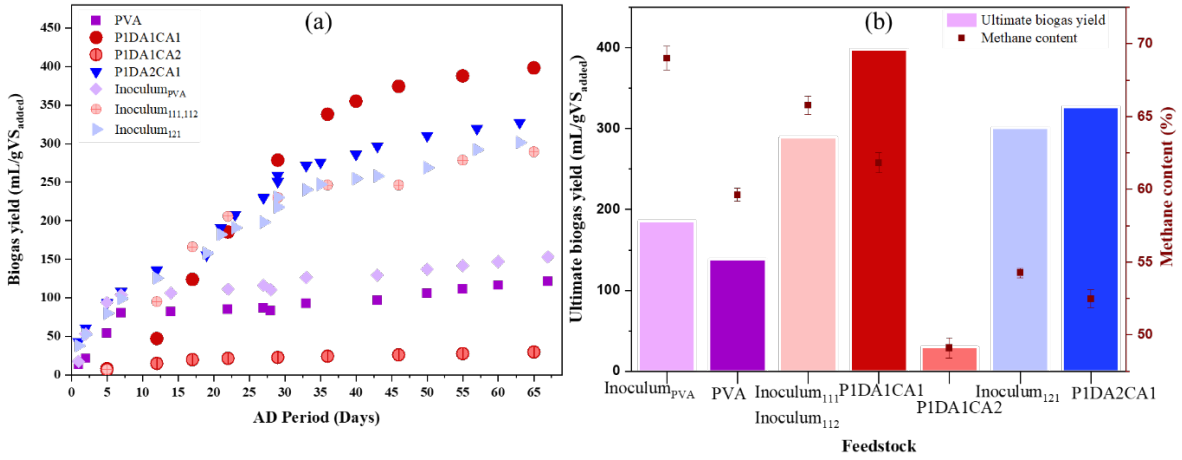


***Fig. 2****. Cumulative biogas yield (a), and ultimate biogas yield and methane content (b) of four different type of plastics (PVA, P1DA1CA1, P1DA2CA1, and P1DA1CA2) and the inoculum.*

Three distinct phenomena were observed in the AD of conventional plastic (PVA) and modified plastics (P1DA1CA1, P1DA2CA1, and P1DA1CA2). First, the lag phase, the biogas production started immediately from the day 1 of AD for all samples except for the modified plastic sample P1DA1CA1. Among the studied samples the highest biogas production during lag phase was found for modified plastic. AD of conventional plastic (PVA) had lower lag phase of 0.2 day than the modified plastics (6.5 days for P1DA1CA1, 0.4 day P1DA2CA1, and 2 days for P1DA1CA2). The longer lag phase in modified plastics is potentially due to the release of different acids used in its preparation, which resulted in a decreased pH in the samples. Methanogens could experience a decrease in their function activity, leading to a noteworthy decline in methane production in AD when exposed to elevated acidic levels [3,4]. Second, the cumulative biogas production rate increased after the lag phase but a rapid biogas

yield was noted for P1DA1CA1 (16.7 mL/g VS. d) and PVA (16.4 mL/g VS. d) followed by P1DA2CA1 (11.7 mL/g VS. d) and P1DA1CA2 (1.8 mL/g VS. d). The higher rate of biogas production in modified plastic P1DA1CA1 is due to the rapid conversion of organic matter or VFA to biogas. A sharp increase in cumulative biogas yield for P1DA2CA1 and P1DA1CA1 was observed after the 19th day of AD and 12th day of AD. The sharp increase in biogas yield suggests that the hydrolysis had been occurring over these days [5]. Third, the highest ultimate biogas yield was noticed for sample P1DA1CA1 (398 mL/gVSadded) followed by P1DA2CA1 (327 mL/gVSadded), PVA (138 mL/gVSadded) and the lowest ultimate biogas yield was noticed for sample P1DA1CA2 (29.7 mL/gVSadded) (Fig. 2b). Among the four studied samples only in sample P1DA1CA1 and P1DA2CA1 an increase in biogas yield over the control or inoculum was noticed. However, in samples PVA and P1DA1CA2 a decrease in ultimate biogas yield was noticed by a factor of 0.74 and 0.1 compared to the inoculum, respectively. Among all the studied samples, a decrease in methane content over inoculum was noticed throughout the studied period. In the study of Zhang et al., [6], it was found that subjecting feedstock to anaerobic treatment under alkaline conditions led to a substantial improvement in methane production. This suggests that the pH value plays a significant role in influencing methane production and the methane content in biogas within anaerobic digestion systems. The decrease in methane content in AD of different type of polymers is due to the use of different acids in its preparation.

**Table 1**: Summary of results of kinetic parameters and soundness of the logistic function model, Modified Gompertz model, and Transference function model for four different type of plastics (PVA, P1DA1CA1, P1DA1CA2, and P1DA2CA1).

| Feedstock | Ultimate Biogas (mL/g VS) | Logistic Function mode | | | | | Modified Gompertz model | | | | | Transference Function model | | | | |
|---|---|---|---|---|---|---|---|---|---|---|---|---|---|---|---|---|
| | | M (mL/ g VS) | Rm (mL/ g VS. d) | λ ($d^{-1}$) | $R^2$ | RMSE | M (mL/ g VS) | Rm (mL/ g VS. d) | λ ($d^{-1}$) | $R^2$ | RMSE | M (mL/ g VS) | Rm (mL/ g VS. d) | λ ($d^{-1}$) | $R^2$ | RMSE |
| PVA | 121.5 | 110.2 | 2.6 | -13.1 | 0.8245 | 13.1 | 96.3 | 11.9 | 0.1 | 0.9865 | 10.0 | 120.0 | 16.4 | 0.2 | 0.8782 | 19.3 |
| P1DA1CA1 | 398.2 | 15.0 | 10.0 | 8.9 | 0.9965 | 8.9 | 400.0 | 11.0 | 1.0 | 0.9912 | 290.0 | 488.4 | 16.7 | 6.5 | 0.9714 | 23.7 |
| P1DA1CA2 | 29.7 | 27.3 | 0.9 | -4.4 | 0.9488 | 1.5 | 35.0 | 4.8 | 321.9 | 0.9488 | 22.5 | 28.6 | 1.8 | 0.4 | 0.9785 | 1.0 |
| P1DA2CA1 | 327.3 | 328.1 | 7.5 | -4.8 | 0.9887 | 9.5 | 330.0 | 7.6 | 2.0 | 0.9712 | 43.2 | 388.9 | 11.7 | 2.0 | 0.9844 | 35.1 |

**Variation in stability parameters in anaerobic digestion of polymer**. The variation in stability parameters (pH, TS, VS and VFA content) before and after anaerobic digestion is presented in Table 2. The pH plays a vital role in assessing the stability of the AD process and exerts a substantial impact on the acid-forming and methane-producing microorganisms. The initial pH was 7.4 for PVA, 7.54 for P1DA1CA1, 6.33 for P1DA1CA2 and 7.86 for P1DA2CA1. At the end of the AD, final pH values were 7.35 to 7.64. The slight increases in pH in P1DA1CA1 and P1DA2CA1, and the explanation could be the accumulation of the unconsumed fatty acids in the reactor. . The TS content in all samples on a weight basis was > 95 %. VS is the second important parameter after biogas production in addressing effectiveness of AD. A high VS content (>98 % of TS) in all the polymers were noticed. The VS content decreased after AD. The decrease in VS content indicates the conversion of organic matter to biogas. The VFA concentration serves as an indicator of the onset of the acidogenesis reaction and presents a significant hurdle in ensuring the stability of the AD process, as it impacts pH, alkalinity, and the functionality of methanogenic microorganisms. The VFA concentration increased after AD. The increase in VFA concentration indicates the conversion of organic matter into different acids by acidogenic bacteria. Throughout the digestion period, the concentration of VFAs remained below the inhibitory threshold of 8000 mg/L, signifying favorable conditions for the growth and activity of acid-generating microorganisms [7].

**Table 2**: Characteristics of feedstock before and after anaerobic digestion.

| **Parameter** | **PVA** | | **$P_1DA_1CA_1$** | | **$P_1DA_1CA_2$** | | **$P_1DA_2CA_1$** | |
|---|---|---|---|---|---|---|---|---|
| | **Before** | **After** | **Before** | **After** | **Before** | **After** | **Before** | **After** |
| **pH** | 7.4±0.3 | 7.60 | 7.54±0.06 | 7.35 | 6.33±0.08 | 7.545 | 7.86 ± 0.04 | 7.64±0.9 |

| | | | | | | | | |
|---|---|---|---|---|---|---|---|---|
| **Total Solid (TS) (%)** | 98.08±3.7 | 99.4 | 97.12±1.7 | 98.8 | 98.8 | 99.9 | 97.3 | 97.3 |
| **Volatile Solid (% of TS)** | 98.79 | 90.3 | 99.91 | 77.1 | 99.92 | 74.31 | 99.87 | |
| **VFA (mg/L)** | 22.83 | 210 | 478 | 5834 | 323 | 2107 | 140 | 547 |

## 5. Conclusions

We have introduced an economically feasible approach for crafting dopamine (DA) assisted polyvinyl alcohol (PVA) adhesive films, which can be conveniently stored at room temperature without necessitating special conditions. The incorporation of citric acid (CA) as a plasticizer, alongside its role in controlling the oxidation of DA, broadened the application scope of the manufactured films. This paper reports a time-based investigation into the stability of DA in deionized water at various pH levels, offering valuable insights for the prolonged and uncomplicated storage of solutions.By adjusting the concentration of the adhesive component (DA) and the plasticizer (CA), a cost-effective method is established to fine-tune the morphological, thermal, adhesive, mechanical, and biodegradation properties of the composite films. The biodegradability study affirms that, in anaerobic conditions, the most biodegradable polymer is P1DA1CA1, followed by P1DA2CA1, PVA, and P1DA1CA2. These films hold potential applications in electronic sensors, printed circuit boards (PCBs), and as a foundation for 3D-printing sensors. The research underscores significant possibilities for integrating such self-adhesive substrates into everyday electronic applications, warranting further exploration.

**Declaration of competing interest**.

The authors declare no competing financial interest.

**Acknowledgments**.

The work was supported by research grant (37508) from Villum Fonden.

**References**.

Gartiser, S., Wallrabenstein, M., Stiene, G., 1998. Assessment of several test methods for the determination of the anaerobic biodegradability of polymers. J. Environ. Polym. Degrad. 6, 159–173.

Matsumura, S., Kurita, H., Shimokobe, H., 1993. Anaerobic biodegradability of polyvinyl alcohol. Biotechnol. Lett. 15, 749–754.

Matsumura, S., Tanaka, T., 1994. Novel malonate-type copolymers containing vinyl alcohol blocks as biodegradable segments and their builder performance in detergent formulations. J. Environ. Polym. Degrad. 2, 89–97.

Mohee, R., Unmar, G.D., Mudhoo, A., Khadoo, P., 2008. Biodegradability of biodegradable/degradable plastic materials under aerobic and anaerobic conditions. Waste Manag. 28, 1624–1629.

Russo, M.A.L., O'Sullivan, C., Rounsefell, B., Halley, P.J., Truss, R., Clarke, W.P., 2009. The anaerobic degradability of thermoplastic starch: Polyvinyl alcohol blends: Potential biodegradable food packaging materials. Bioresour. Technol. 100, 1705–1710. https://doi.org/https://doi.org/10.1016/j.biortech.2008.09.026

Sitthi, S., Hatamoto, M., Watari, T., Yamaguchi, T., 2022. Accelerating anaerobic propionate degradation and studying microbial community using modified polyvinyl alcohol beads during anaerobic digestion. Bioresour. Technol. Reports 17, 100907. https://doi.org/https://doi.org/10.1016/j.biteb.2021.100907

Zhang, D., Chen, Y., Zhao, Y., Zhu, X., 2010. New sludge pretreatment method to improve methane production in waste activated sludge digestion. Environ. Sci. Technol. 44, 4802–4808.

1. Kizilkan Eand Gorb S N, 2018, Bioinspired Further Enhanced Dry Adhesive by the Combined Effect of the Microstructure and Surface Free-Energy Increase. ACS Applied Materials & Interfaces, 10(31): 26752-26758. 10.1021/acsami.8b06686

2. Hosoda N, Nakamoto M, Suga T, et al., 2021, Evidence for intermolecular forces involved in ladybird beetle tarsal setae adhesion. Scientific Reports, 11(1): 7729. 10.1038/s41598-021-87383-9

3. Molina Lopez J F, Rojas Garcia P P, Szydlo-Shein G, et al., 2014, Use of n-Butyl-2 cyanoacrylate for closure of large fasciocutaneous abdominal skin flaps: an experimental model. Journal of the American College of Surgeons, 219(4): e137. 10.1016/j.jamcollsurg.2014.07.752

4. Liu H, Yuan M, Sonamuthu J, et al., 2020, A dopamine-functionalized aqueous-based silk protein hydrogel bioadhesive for biomedical wound closure. New Journal of Chemistry, 44(3): 884-891. 10.1039/C9NJ04545G

5. Waite J Hand Tanzer M L, 1981, Polyphenolic Substance of Mytilus edulis: Novel Adhesive Containing L-Dopa and Hydroxyproline. Science, 212(4498): 1038-1040. doi:10.1126/science.212.4498.1038

6. Lee H, Dellatore S M, Miller W M, et al., 2007, Mussel-Inspired Surface Chemistry for Multifunctional Coatings. Science, 318(5849): 426-430. doi:10.1126/science.1147241

7. Wei Q, Zhang F, Li J, et al., 2010, Oxidant-induced dopamine polymerization for multifunctional coatings. Polymer Chemistry, 1(9): 1430-1433. 10.1039/C0PY00215A
8. Zhang Z, Gao Z, Wang Y, et al., 2019, Eco-Friendly, Self-Healing Hydrogels for Adhesive and Elastic Strain Sensors, Circuit Repairing, and Flexible Electronic Devices. Macromolecules, 52(6): 2531-2541. 10.1021/acs.macromol.8b02466
9. Li Fand Xia H, 2017, Dopamine-functionalized poly(vinyl alcohol) elastomer with melt processability and self-healing properties. Journal of Applied Polymer Science, 134(28): 45072. https://doi.org/10.1002/app.45072
10. Sousa M Pand Mano J F, 2017, Cell-Adhesive Bioinspired and Catechol-Based Multilayer Freestanding Membranes for Bone Tissue Engineering. Biomimetics, 2(4): 19.
11. Han L, Yan L, Wang K, et al., 2017, Tough, self-healable and tissue-adhesive hydrogel with tunable multifunctionality. NPG Asia Materials, 9(4): e372-e372. 10.1038/am.2017.33
12. Zhang C, Zhou Y, Han H, et al., 2021, Dopamine-Triggered Hydrogels with High Transparency, Self-Adhesion, and Thermoresponse as Skinlike Sensors. ACS Nano, 15(1): 1785-1794. 10.1021/acsnano.0c09577
13. Qian B, Zheng Z, Michailids M, et al., 2019, Mussel-Inspired Self-Healing Coatings Based on Polydopamine-Coated Nanocontainers for Corrosion Protection. ACS Applied Materials & Interfaces, 11(10): 10283-10291. 10.1021/acsami.8b21197
14. Wang X-T, Deng X, Zhang T-D, et al., 2022, A Versatile Hydrophilic and Antifouling Coating Based on Dopamine Modified Four-Arm Polyethylene Glycol by One-Step Synthesis Method. ACS Macro Letters, 11(6): 805-812. 10.1021/acsmacrolett.2c00277
15. Asha A B, Peng Y-Y, Cheng Q, et al., 2022, Dopamine Assisted Self-Cleaning, Antifouling, and Antibacterial Coating via Dynamic Covalent Interactions. ACS Applied Materials & Interfaces, 14(7): 9557-9569. 10.1021/acsami.1c19337
16. Hu P, Xie R, Xie Q, et al., 2022, Simultaneous realization of antifouling, self-healing, and strong substrate adhesion via a bioinspired self-stratification strategy. Chemical Engineering Journal, 449: 137875. https://doi.org/10.1016/j.cej.2022.137875
17. Putnam A Aand Wilker J J, 2021, Changing polymer catechol content to generate adhesives for high versus low energy surfaces. Soft Matter, 17(7): 1999-2009. 10.1039/D0SM01944E
18. Panchireddy S, Grignard B, Thomassin J-M, et al., 2018, Catechol Containing Polyhydroxyurethanes as High-Performance Coatings and Adhesives. ACS Sustainable Chemistry & Engineering, 6(11): 14936-14944. 10.1021/acssuschemeng.8b03429
19. Zhang W, Wang R, Sun Z, et al., 2020, Catechol-functionalized hydrogels: biomimetic design, adhesion mechanism, and biomedical applications. Chemical Society Reviews, 49(2): 433-464. 10.1039/C9CS00285E
20. Gan D, Xing W, Jiang L, et al., 2019, Plant-inspired adhesive and tough hydrogel based on Ag-Lignin nanoparticles-triggered dynamic redox catechol chemistry. Nature Communications, 10(1): 1487. 10.1038/s41467-019-09351-2
21. Lee H, Scherer N Fand Messersmith P B, 2006, Single-molecule mechanics of mussel adhesion. Proceedings of the National Academy of Sciences, 103(35): 12999-13003. doi:10.1073/pnas.0605552103
22. Chen T-P, Liu T, Su T-L, et al., 2017, Self-Polymerization of Dopamine in Acidic Environments without Oxygen. Langmuir, 33(23): 5863-5871. 10.1021/acs.langmuir.7b01127
23. Kim J, Lee Cand Ryu J H, 2021, Adhesive Catechol-Conjugated Hyaluronic Acid for Biomedical Applications: A Mini Review. Applied Sciences, 11(1): 21.
24. Lopezcarasa-Hernandez G, Perez-Vazquez J-F, Guerrero-Naranjo J-L, et al., 2021, Versatility of use of fibrin glue in wound closure and vitreo-retinal surgery. International Journal of Retina and Vitreous, 7(1): 33. 10.1186/s40942-021-00298-5

25. Ji Y, Ji T, Liang K, et al., 2015, Mussel-inspired soft-tissue adhesive based on poly(diol citrate) with catechol functionality. Journal of Materials Science: Materials in Medicine, 27(2): 30. 10.1007/s10856-015-5649-2
26. Krogsgaard M, Nue Vand Birkedal H, 2016, Mussel-Inspired Materials: Self-Healing through Coordination Chemistry. Chemistry – A European Journal, 22(3): 844-857. https://doi.org/10.1002/chem.201503380
27. Yang W J, Xu W, Tao X, et al., 2020, Two-stage thiol-based click reactions for the preparation and adhesion of hydrogels. Polymer Chemistry, 11(17): 2986-2994. 10.1039/C9PY01503E
28. Bonafé Allende J C, Schmarsow R N, Matxinandiarena E, et al., 2022, Crystallization-Driven Supramolecular Gelation of Poly(vinyl alcohol) by a Small Catechol Derivative. Macromolecules, 55(24): 10870-10879. 10.1021/acs.macromol.2c01364
29. Fan L, Xie J, Zheng Y, et al., 2020, Antibacterial, Self-Adhesive, Recyclable, and Tough Conductive Composite Hydrogels for Ultrasensitive Strain Sensing. ACS Applied Materials & Interfaces, 12(19): 22225-22236. 10.1021/acsami.0c06091
30. Shi D, Liu R, Dong W, et al., 2015, pH-dependent and self-healing properties of mussel modified poly(vinyl alcohol) hydrogels in a metal-free environment. RSC Advances, 5(100): 82252-82258. 10.1039/C5RA15991A
31. Yu M, Hwang Jand Deming T J, 1999, Role of l-3,4-Dihydroxyphenylalanine in Mussel Adhesive Proteins. Journal of the American Chemical Society, 121(24): 5825-5826. 10.1021/ja990469y
32. Du X, Li L, Behboodi-Sadabad F, et al., 2017, Bio-inspired strategy for controlled dopamine polymerization in basic solutions. Polymer Chemistry, 8(14): 2145-2151. 10.1039/C7PY00051K
33. Du X, Li L, Li J, et al., 2014, UV-Triggered Dopamine Polymerization: Control of Polymerization, Surface Coating, and Photopatterning. Advanced Materials, 26(47): 8029-8033. https://doi.org/10.1002/adma.201403709
34. Liu Y, Ai Kand Lu L, 2014, Polydopamine and Its Derivative Materials: Synthesis and Promising Applications in Energy, Environmental, and Biomedical Fields. Chemical Reviews, 114(9): 5057-5115. 10.1021/cr400407a
35. Zhang C, Ou Y, Lei W-X, et al., 2016, CuSO4/H2O2-Induced Rapid Deposition of Polydopamine Coatings with High Uniformity and Enhanced Stability. Angewandte Chemie International Edition, 55(9): 3054-3057. https://doi.org/10.1002/anie.201510724
36. Zheng W, Fan H, Wang L, et al., 2015, Oxidative Self-Polymerization of Dopamine in an Acidic Environment. Langmuir, 31(42): 11671-11677. 10.1021/acs.langmuir.5b02757
37. Hong S, Wang Y, Park S Y, et al., 2018, Progressive fuzzy cation-π assembly of biological catecholamines. Science Advances, 4(9): eaat7457. doi:10.1126/sciadv.aat7457
38. Assender H Eand Windle A H, 1998, Crystallinity in poly(vinyl alcohol). 1. An X-ray diffraction study of atactic PVOH. Polymer, 39(18): 4295-4302. https://doi.org/10.1016/S0032-3861(97)10296-8
39. El-Shamy A G, Attia Wand Abd El-Kader K M, 2014, The optical and mechanical properties of PVA-Ag nanocomposite films. Journal of Alloys and Compounds, 590: 309-312. https://doi.org/10.1016/j.jallcom.2013.11.203
40. Li Y, Fang X, Wang Y, et al., 2016, Highly Transparent and Water-Enabled Healable Antifogging and Frost-Resisting Films Based on Poly(vinyl alcohol)–Nafion Complexes. Chemistry of Materials, 28(19): 6975-6984. 10.1021/acs.chemmater.6b02684

41. Agubata C O, Mbah M A, Akpa P A, et al., 2021, Application of self-healing, swellable and biodegradable polymers for wound treatment. Journal of Wound Care, 30(Sup9a): IVi-IVx. 10.12968/jowc.2021.30.Sup9a.IV
42. Zhang Xand He J, 2015, Hydrogen-Bonding-Supported Self-Healing Antifogging Thin Films. Scientific Reports, 5(1): 9227. 10.1038/srep09227
43. Chen M, Wu Y, Chen B, et al., 2022, Fast, strong, and reversible adhesives with dynamic covalent bonds for potential use in wound dressing. Proceedings of the National Academy of Sciences, 119(29): e2203074119. doi:10.1073/pnas.2203074119

**Graphical Abstract:**